

1 Introduction

LHC has recently reported the discovery of a Higgs boson [1, 2]. The properties of this newly found particle, so far, strongly resemble the properties of the Standard Model (SM) Higgs [3, 4]. However, the task of fully establishing the nature of the electroweak symmetry breaking is far from completion. One of the ways to test the properties of the newly discovered field is to compare its couplings to the SM predictions. The current data shows agreement between theory and experiments of the order of 20% – 30% [3, 4]. It should be noted that the constraints on the values of the Higgs top Yukawa coupling come mainly from the gluon fusion measurements and the constraints from the associated production of Higgs with a top pair are still weak [5–7]. The discrepancies between Higgs top Yukawa coupling and the gluon fusion rate can easily arise in theories beyond the Standard Model, where the scale of the electroweak symmetry breaking is natural. Indeed, the majority of these models predict new states, which are charged under the SU(3) colour gauge group and interact with the Higgs boson. It is plausible that these states are beyond the direct production reach at LHC energies, however their indirect effects can show up in the modifications of the Higgs couplings. At low energies, modifications of the Higgs couplings to gluons and top quarks can be parametrized as

$$\mathcal{L} = -c_t \frac{m_t}{v} \bar{t} t h + \frac{g_s^2}{48\pi^2} c_g \frac{h}{v} G_{\mu\nu} G^{\mu\nu}, \quad (1.1)$$

where the $(c_t = 1, c_g = 0)$ point corresponds to the SM. We have normalized the Higgs interaction with gluons in a way that $c_g = 1$ corresponds to the operator generated by an infinitely heavy top quark. Single Higgs production occurs at the scale $m_H < m_t$ so that the Higgs Low Energy Theorems [8, 9] are applicable and the effective operator controlling the Higgs couplings to gluons will be given by

$$O_g(m_H) \approx \frac{g_s^2}{48\pi^2} (c_g + c_t) \frac{h}{v} G_{\mu\nu} G^{\mu\nu}. \quad (1.2)$$

Eq. 1.2 shows that the overall gluon fusion rate will be proportional to $|c_g + c_t|$ and there is no way to disentangle this combinations of the Higgs couplings from the gluon fusion process only. The current fit of these couplings is given in Fig. 1. We can see that the current data is peaked along the $c_t + c_g = \text{const}$ line. The black contours surrounding the

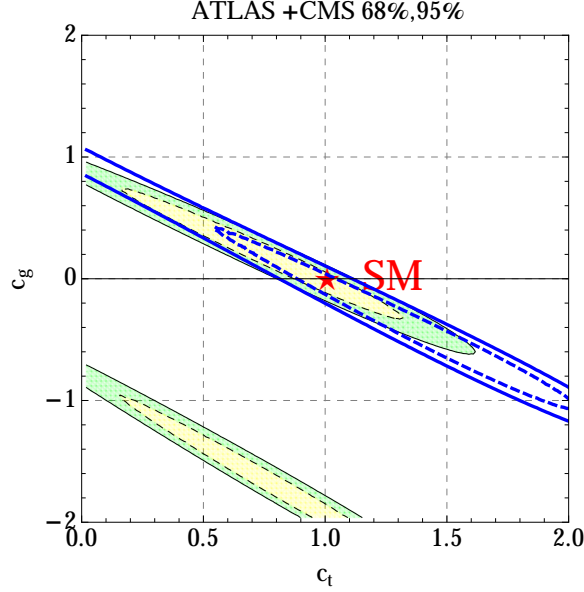


Figure 1: 68% and 95% (yellow and green) probability contours in the (c_t, c_g) plane from the Higgs couplings (based on the Lagrangian Eq.1.1). The red star indicates Standard Model. Blue lines correspond to the 68% and 95% contours for the Lagrangian Eq.1.3.

yellow and green areas indicate 68% and 95% percent probability regions respectively. The fit was obtained using the likelihood from [10]² and assuming that the only deviations of the Higgs couplings are the ones in the Lagrangian in Eq. 1.1. We can see that there is a strong degeneracy in probability contours along the $c_t + c_g = \text{const}$ direction. The only channels that break this degeneracy are $h \rightarrow \gamma\gamma$ and $pp \rightarrow t\bar{t}h \rightarrow t\bar{t}(b\bar{b}, \gamma\gamma, WW, ZZ, \tau\tau)$. However the discriminating power of the $h \rightarrow \gamma\gamma$ channel is weak because the Higgs interaction with two photons is dominated by the W loop. The blue dotted and dashed dotted lines on the Fig.1 represent 68% and 95% percent probability regions within the assumption that O_g operator is generated by the fields, which have the same quantum numbers as SM top quarks, i.e., the effective Lagrangian is given by

$$\mathcal{L} = -c_t \frac{m_t}{v} t\bar{t}h + \frac{g_s^2}{48\pi^2} c_g \frac{h}{v} G_{\mu\nu} G^{\mu\nu} + \frac{e^2}{18\pi^2} c_g \frac{h}{v} \gamma_{\mu\nu} \gamma^{\mu\nu}. \quad (1.3)$$

²We have also included a recent CMS analysis [6] with multiplepton final state.

The c_t, c_g degeneracy becomes even stronger in this case since the only channels that break it are ³

$$pp \rightarrow t\bar{t}h \rightarrow t\bar{t}(b\bar{b}, \gamma\gamma, WW, ZZ, \bar{\tau}\tau). \quad (1.4)$$

The second ellipse solution with negative c_g is gone due to the strong constraints on the overall $h \rightarrow \gamma\gamma$ rate, also it is interesting to note that the maximum of the probability is shifted towards values of c_t greater than one due to the recent measurements of the $t\bar{t}h$ interaction in the multilepton final state [6]. In this paper we propose to look at the $pp \rightarrow h+j$ process as another way to resolve this degeneracy⁴. Indeed, at high transverse momentum (p_T), when the center of mass energy becomes larger than the top mass (m_t) and we cannot integrate it out, the cross section becomes proportional to

$$\frac{d\sigma}{dp_T} = \sum_i \kappa_i |f^i(p_T)c_t + c_g|^2, \quad (1.5)$$

$$\left(\frac{d\sigma^{SM}(m_t)}{dp_T}\right) / \left(\frac{d\sigma^{SM}(m_t \rightarrow \infty)}{dp_T}\right) = \frac{\sum_i \kappa_i f^i(p_T)^2}{\sum_i \kappa_i}, \quad (1.6)$$

where the sum is over all non-interfering processes contributing to the $pp \rightarrow h+j$. For example, the recent next to leading order (NLO) calculation predicts [13]

$$\left(\frac{d\sigma^{SM}(m_t)}{dp_T}\right) / \left(\frac{d\sigma^{SM}(m_t \rightarrow \infty)}{dp_T}\right) \Big|_{p_T=300\text{GeV}} \sim 0.7. \quad (1.7)$$

Hence the measurements of the Higgs production at high p_T can shed light on the c_t and c_g couplings.

Lastly, we would like to comment that the (c_t, c_g) degeneracy is manifest in the Composite Higgs models [14], where the $c_t + c_g$ combination of the Higgs couplings constants was shown to be independent of the details of the spectrum of composite resonances [15]⁵.

³For the latest studies on the measurements of the top Yukawa couplings from the $pp \rightarrow th, pp \rightarrow t\bar{t}h$ processes see [11]

⁴Recently the same process was proposed for the studies of the dimension 7 operators for the Higgs gluon interactions [12].

⁵While this work was at the stage of completion, a similar proposal to use $h+j$ at high p_T to resolve the (c_t, c_g) degeneracy and extract information about the spectrum of composite resonances was suggested in the context of the Composite Higgs and Little Higgs scenarios [16].

2 Cross section as a function of (c_t, c_g)

The dominant processes contributing to the $pp \rightarrow h+j$ at the parton level are $gg \rightarrow gh, qq \rightarrow qh, \bar{q}q \rightarrow \bar{q}h$. The contribution from $q\bar{q} \rightarrow h+g$ is subleading by orders of magnitude. At the leading order (LO) the matrix elements for the loops of the top quarks were calculated by [17, 18]. These can be easily recasted into the (c_t, c_g) plane using the relation

$$M_i(c_t, c_g) = c_t M_i(m_t) + c_g M_i(m_t \rightarrow \infty). \quad (2.8)$$

We used LoopTools [19] to compute the Passarino-Veltman loop functions appearing in the matrix elements $M_i(m_t)$. The isocontours of $|M_i|^2$ are shown in Fig. 2. We can see that at high collision energy the shapes of the isocontours are changed. Note that for $M_{q\bar{q} \rightarrow gh}$ the isocontours are no more the straight lines because there is a large imaginary part corresponding to the real top pair production with the gluon in the S channel.

Before proceeding further we would like to comment on the validity of the effective field theory (EFT) approach for parametrization of the new physics (NP) contribution in terms of the Lagrangian in Eq.1.1. We have checked numerically that, when O_g is generated by the loops of new fermions, effective field theory still provides a good description of the physics if the energy of the collision is below

$$\sqrt{s} \lesssim \mathcal{O}(M_{NF}), \quad (2.9)$$

where M_{NF} is the mass of the new fermion⁶ and we can use this inequation as an estimate of the EFT validity range.

The partonic cross section is convoluted into the hadronic one using the procedure described in [20]⁷, and using the PDF sets provided by MSTW2008 [23].

$$d\sigma(pp \rightarrow hj) = \sum_{ab} f(x_1)f(x_2)dx_1dx_2 \sum |M(ab \rightarrow h+j)|^2 (2\pi)^4 \times \delta^4(p_1 + p_2 - p_H - p_j) \frac{d^3p_H}{2(2\pi)^3 E_H} \frac{d^3p_j}{2(2\pi)^3 E_j}. \quad (2.10)$$

⁶The exact upper bound on \sqrt{s} depends on the contributing subprocess and for $gg \rightarrow gh, (qq \rightarrow qh, q\bar{q} \rightarrow gh)$ is equal to $\sqrt{s} \lesssim 1.7, (1, 0.7)M_{NF}$ respectively.

⁷In this regards the works [21] and [22] prove very useful too.

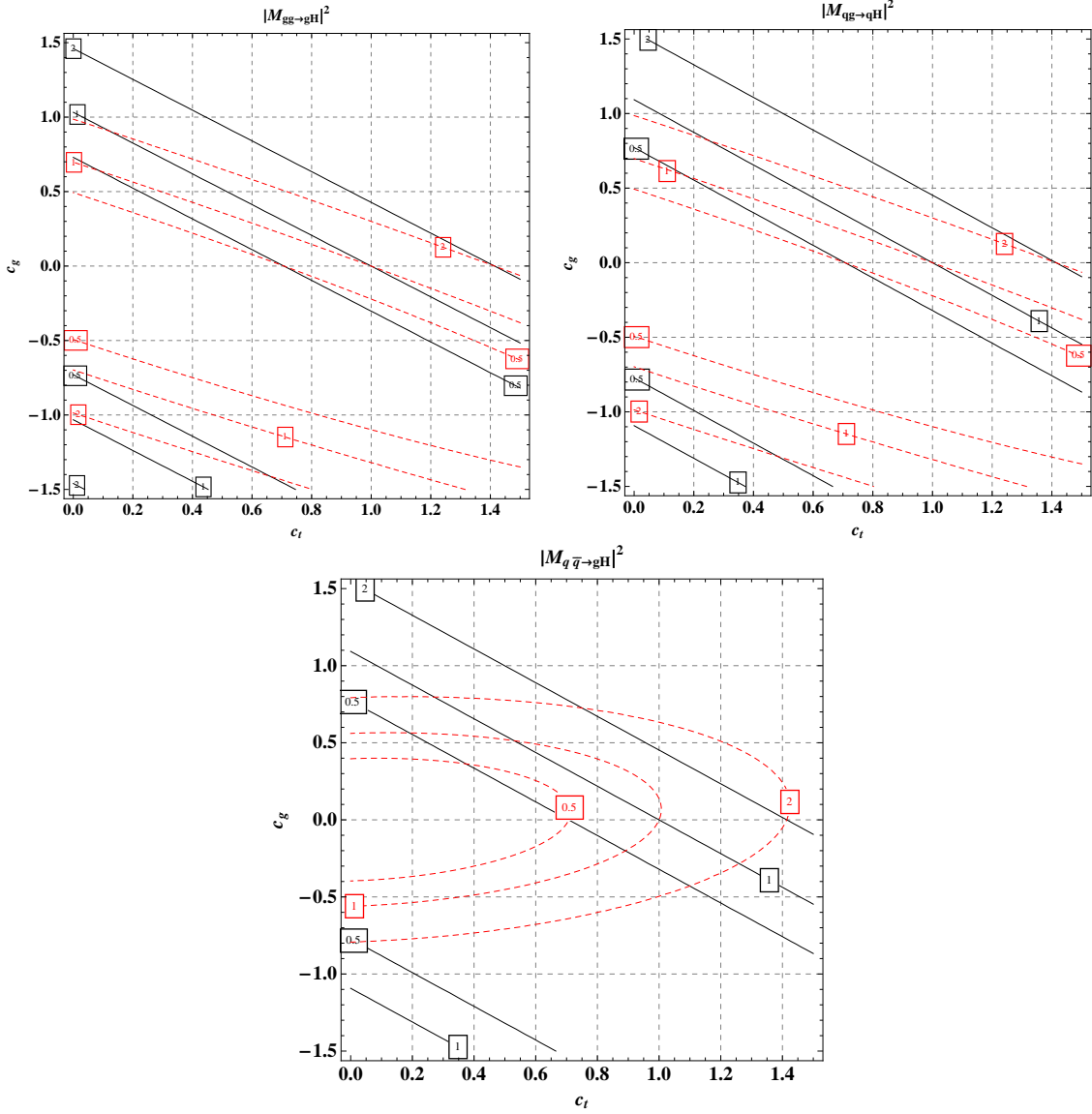


Figure 2: Isocontours of $|M_i|^2$ for various values of \hat{s} , $\hat{t} = \hat{u} = (m_H^2 - \hat{s})/2$. The red dashed line corresponds to the $\sqrt{\hat{s}} = 1000$ GeV and the black solid line to the $\sqrt{\hat{s}} = 130$ GeV. Contour labels indicate modification of the $|M_i|^2$ compared to the SM expectations.

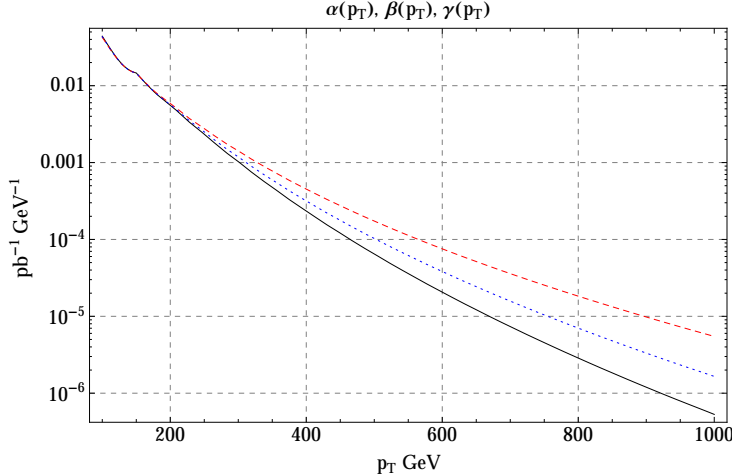


Figure 3: Coefficients α, β, γ as a functions of p_T . Black (solid) – $\alpha(p_T)$, blue (dotted) – $\gamma(p_T)$, red (dashed) – $\beta(p_T)$, for the center of mass energy $\sqrt{S} = 14$ TeV.

The LO overall cross section is a second order polynomial of the coefficients c_t and c_g

$$\frac{d\sigma}{dp_T} = \alpha(p_T)c_t^2 + \beta(p_T)c_g^2 + 2\gamma(p_T)c_t c_g. \quad (2.11)$$

We present the values of the coefficients $\alpha(p_T)$, $\beta(p_T)$ and $\gamma(p_T)$ for the various values of p_T in Fig 3. As expected, the difference between these coefficients grows with p_T . During our calculation we have set the renormalization and the factorization scales at

$$\mu_r = \mu_f = \sqrt{p_T^2 + m_H^2}. \quad (2.12)$$

To take into account higher order NLO QCD corrections we have calculated the $K(p_T)$ factors using HqT ⁸ [24], and for this choice of the renormalization and factorization scale K factors are roughly p_T independent and are approximately $K(p_T) \sim 2$. We have also verified that the resummation effects are negligible in the p_T range we have considered. Isocontours of the differential cross section in the (c_t, c_g) plane are shown in Fig 4, we can see that they strongly resemble the isocurves of the matrix elements, since the subprocess $q\bar{q} \rightarrow gH$ is strongly subleading.

⁸While HqT provides the LO+NLL and NLO+NNLL estimates, the LO estimates are not implemented with the Passarino-Veltman loop functions and hence break down at high p_T .

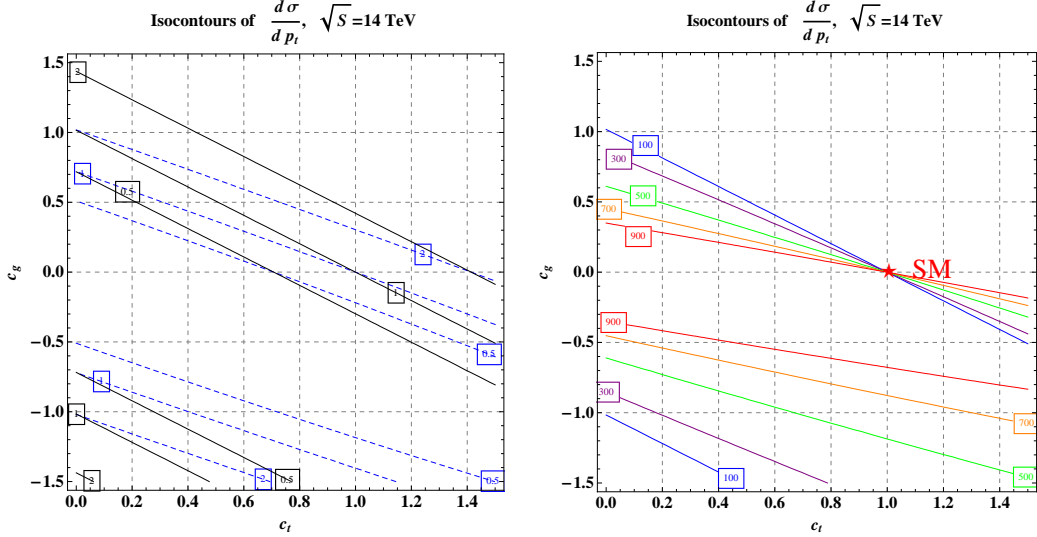


Figure 4: Left – Isocontours of $\frac{d\sigma}{dp_T}$ in the units of the SM differential cross section. Blue (dashed) – $p_T = 400\text{GeV}$, black (solid) – $p_T = 100\text{ GeV}$, SM corresponds to the (1,0) point in the plane. Right – isocontours of the SM cross section for various p_T in GeV(indicated by the labels).

Measurement of the cross section at fixed p_T will constrain the plane to a line (band). Combining measurements at various p_T (intersection of the bands) will fix the Higgs coupling parameters c_t, c_g . Ideally, the whole p_T distribution of all the events should be used to reconstruct the c_t, c_g coefficients of the effective Lagrangian. However, to simplify the analysis and to estimate the LHC potential for c_t, c_g measurements in the $pp \rightarrow h + j$ analysis, we can categorize all the events into two bins with high and low p_T .

$$\begin{aligned}
 \sigma^-(p_T < P_T) &= \int_{p_T^{\min}}^{P_T} \frac{d\sigma}{dp_T} dp_T, & N^- &= \sigma^- \times \text{Luminosity}, \\
 \sigma^+(p_T > P_T) &= \int_{P_T}^{p_T^{\max}} \frac{d\sigma}{dp_T} dp_T, & N^+ &= \sigma^+ \times \text{Luminosity},
 \end{aligned}
 \tag{2.13}$$

where N^\pm are number of events seen in the respective bins. Calculating the real SM background is beyond the scope of this paper, so to roughly estimate the LHC potential at 14 TeV at very high luminosity we decided to look at the Higgs decays into the four lepton final mode $h \rightarrow ZZ^* \rightarrow l^-l^-l^+l^+$ and estimated the background at the partonic level using [25]. We assume Bayesian statistics and treat the scale and PDF uncertainties as systematic er-

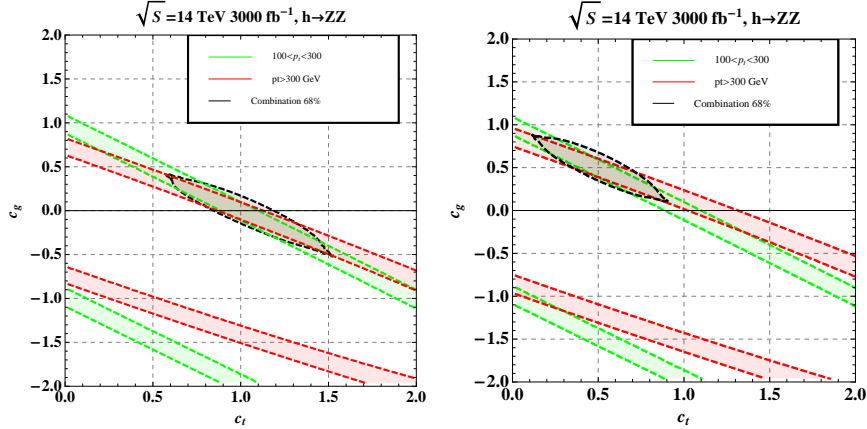


Figure 5: Green – 68% band coming from the N^- measurement, red – 68% band coming from the N^+ measurement for $P_T = 300$ GeV. Black is a combination assuming 100% correlation between theoretical errors. The probability contours are obtained in Bayesian analysis assuming zero background for $3000 fb^{-1}$. We can see that we need very high luminosity to overcome statistical uncertainty. Left plot corresponds to the SM signal ($c_t = 1, c_g = 0$), right plot to ($c_t = 0.5, c_g = 0.5$).

errors, which are 100% correlated for the N^+ and N^- measurements. The results are shown in the Fig. 5, where the plots are shown for the discriminating momenta $P_T = 300$ GeV. The green band corresponds to the 68% probability contour of the N^- observable. We have treated the choice of renormalization scale and the uncertainty in the PDF as theoretical errors and varied the expected signal within this range with a Gaussian prior. The red contour is a similar band for the N^+ observable. The black contour is a combination assuming hundred percent correlation of the systematic errors which are, in our case, the choice of the renormalization/factorization scale and PDF. Due to this correlation the overall combination contour is not just a simple overlap of the N^\pm contours. However we are dominated by the low p_T measurements, because the statistical uncertainty is much smaller there. We have chosen the two categories to be discriminated by the $P_T = 300$ GeV to have larger number of events in the high p_T category, even though the separation between N^+ and N^- isocurves is small. With $3000 fb^{-1}$ data we have $N^- \sim 60$ events for the SM point.

3 Understanding theory uncertainties

The combined theoretical error in the LO estimate is approximately 50% and that at NLO is approximately 25%. Theory uncertainties come from three sources.

Choice of renormalization and factorization scale:

There are different prescriptions for the choice these scales. The one which is used more prevalently for low p_T analyses is proportional to the Higgs mass, $\mu_r = \mu_f = xm_H$. The other choice is proportional to the transverse energy of the Higgs, $\mu_r = \mu_f = x\sqrt{m_H^2 + p_T^2}$ with x being varied between 0.5 and 2 in general. This is more relevant for high p_T as it is better motivated as the “scale” of the physics process, hence we use it in our work. The other prescription mentioned in the literature [16] is $\mu_r = \mu_f = \frac{x}{2} \left[p_T + \sqrt{m_H^2 + p_T^2} \right]$ which reduces to the latter prescription in the p_T region away from m_H . For the LO cross section, the error from the variation of the scale leads to an error of the same order as the cross section itself. However, at the NLO, this error drops to about 25%. We have checked this using HqT in the infinite top mass limit.

PDF errors:

The PDF errors are of the order of 5%. We used the 68% C.L. sets in the MSTW2008 PDF grids to determine this. Considering the scale error, this error is sub-dominant.

K factor:

Since the NLO calculations have been performed only for an effective infinitely heavy top mass contribution, the K factor for the finite top mass contribution needs to be estimated from the former. Although finite mass effects in the K factor can be expected to be not very large, commenting on the significance of the same is beyond the scope of this work. The variation of the K factor with the choice of scale is of $O(10\%)$, which we have numerically checked using HqT in the infinite top mass limit.

The determination of the c_t, c_g suffers from the systematic errors due to these uncertainties in the theoretical calculation. The scale dependence of the integrated cross sections σ^+ and σ^- comes from the renormalization scale dependence of the strong coupling constant

and the factorizations scale dependence of the PDFs. It is quite clear that the former is multiplicative and will partially drop out in ratios of any differential or partial cross sections. The factorization scale dependence is not so trivial as it comes from a convolution of the PDFs with the partonic amplitudes. However, as long as two partonic contributions are not widely different functionally and numerically, the dependence is approximately multiplicative and can be expected to bring about weak scale dependence in ratios of cross sections. For example, lets look at the ratios

$$R_+ = \frac{\sigma^+}{\sigma_{SM}^+} \quad \text{and} \quad R_- = \frac{\sigma^-}{\sigma_{SM}^-}, \quad (3.14)$$

where σ_{SM}^\pm is defined by setting $c_t = 1$ and $c_g = 0$. In the absence of new physics contributions both these ratios are equal to unity. We have scanned the values of the theoretical errors in the (c_t, c_g) plane and we have found out that the error on the R_+, R_- is always less than 2%, which primarily comes from the convolution of the pdfs in the different p_t regions. It is clear that in both the low p_T (100 - 300 GeV) and the high p_T (300 - 1000 GeV) regions, these ratios are almost independent of the choice of renormalization and factorization scales within the range of variation of the latter that we have chosen and almost independent of PDF errors. This statement is true regardless of what prescription we set for the choice of the scales, i.e., whether we chose fixed scales or running scales. This has a very important implication in the light of the theoretical uncertainties that shroud the calculation of cross sections in this channel. The approximate independence of the ratio from scale choice along with approximate scale (and p_T) independence of the K factor, which are also blind to SM vs. NP contributions, implies that the ratios R^+ and R^- are more or less independent of the order of the theoretical computation and the choice of scales. These ratios can be easily calculated at LO and will be the same even when higher order terms are added to the cross section. Note that both R_+ and R_- are theoretical constructs and do not have any implementations as experimental observables.

3.1 Defining and interpreting r_\pm

We define the ratio

$$r_\pm = \frac{R_+}{R_-}. \quad (3.15)$$

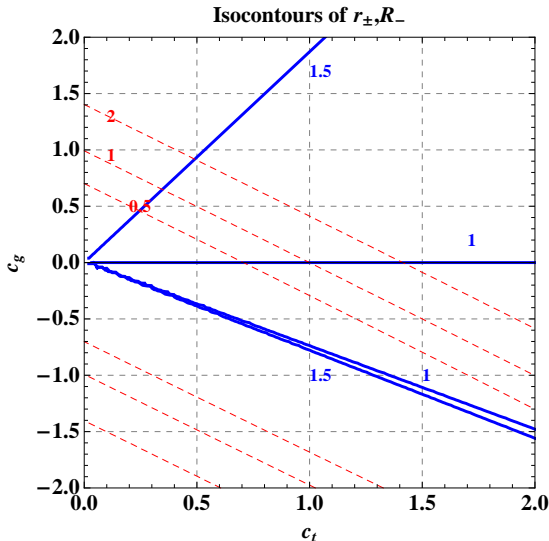


Figure 6: R_{\pm} (red, dashed) and r_{\pm} (blue, solid) contours in the (c_t, c_g) plane, $\sqrt{S} = 14\text{TeV}$, R_{\pm} and r_{\pm} are defined for discriminating momentum $P_T = 300$ GeV.

In the absence of NP contributions $r_{\pm} = 1$. Even in the presence of NP contribution r_{\pm} can be equal to unity if both low p_T and high p_T amplitudes are equivalently enhanced or diminished by NP. However, $r_{\pm} \neq 1$ is a sure sign of the presence of a new degree of freedom and hence can be used as a discriminant from SM.

In the Fig. 6 we show the isocontours of r_{\pm} in the (c_t, c_g) plane. As one can see, there are significant parts of the (c_t, c_g) space where one of R_+ or R_- is diminished from unity while the other is enhanced heralding a presence of the heavy top partner. We have checked numerically that r_{\pm} is almost independent of the PDF choice as well as the renormalization/factorization scale choice. Also, note that the isocontours of the r_{\pm} variable intercept with and are sometimes almost orthogonal to the $\frac{d\sigma}{dp_T}$ contours as can be seen from Fig. 6, which illustrates that r_{\pm} has good discriminating powers in the (c_t, c_g) plane.

As an experimental observable r_{\pm} can be expressed as

$$r_{\pm} = \frac{N^+/N^-}{\sigma_{SM}^+/\sigma_{SM}^-}, \quad (3.16)$$

where N^{\pm} is the number of events seen in respective bins. The denominator suffers from theoretical errors from the choice of scale and PDF errors but is independent of the K factor and we have checked that the overall error is always $\lesssim 10\%$. This means that a LO estimate

is sufficient for evaluating the denominator. The numerator suffers from experimental errors only. This ratio provides a definitive prescription for comparing an experimental measurement with a theoretical predictions with clearly delineated and disentangled experimental and theoretical errors.

4 Conclusion

We will conclude by recapitulating the main results of our work. The current data on the Higgs coupling shows a strong degeneracy in the best fit solutions for the Higgs couplings in the (c_t, c_g) space. In this work we propose to use the $pp \rightarrow h + j$ process to resolve this degeneracy. Indeed the Higgs interaction with gluons generated by the loops of the SM top quark and the dimension five operator have different p_T dependence and this can be used to measure the effective Higgs couplings to tops and gluons. To estimate the LHC potential we have looked at the 4 lepton final state. Due to the very small rate of the signal this measurement can become possible only with very high luminosity at the LHC. The expected constraints on c_t look, so far, inferior compared to the prospects in the direct measurements of the $t\bar{t}h$ coupling [11](ATLAS projections for the 3000 fb⁻¹ predict the determination of the top Yukawa coupling with a $\sim 10\%$ accuracy [26]). However $h + j$ can be used to reduce errors on the c_g coupling when combined with the c_t measurements from $t\bar{t}h$ production. Exploring other Higgs decay final states can also largely increase the precision of the (c_t, c_g) measurements.

We also propose an observables with reduced theoretical errors, r_{\pm} , which can be used as alternative discriminant of NP signal. We show that theoretical and experimental errors can be disentangled in r_{\pm} .

When this work was at the stage of completion we became aware of another project, which also uses $pp \rightarrow h + j$ to measure Higgs couplings [27].

Acknowledgments

We would like to thank S. Rychkov and R. Contino for suggesting the project. We would also like to thank R. Contino for discussions and encouragement throughout the completion of this

work and J. de Blas, M. Son and L. Silvestrini for useful discussions. A. P. would like to thank the Physics Department of the University of Notre Dame du Lac for providing computational resources and hosting him over the summer of 2013 while this work was being done. The work of A. A. was supported by the ERC Advanced Grant No. 267985 *Electroweak Symmetry Breaking, Flavour and Dark Matter: One Solution for Three Mysteries (DaMeSyFla)*. The work of A. P. was supported by the European Research Council under the European Union's Seventh Framework Programme (FP/2007-2013) / ERC Grant Agreement n. 279972.

References

- [1] G. Aad *et al.* [ATLAS Collaboration], Phys. Lett. B **716**, 1 (2012) [[arXiv:1207.7214](#) [[hep-ex](#)]].
- [2] S. Chatrchyan *et al.* [CMS Collaboration], Phys. Lett. B **716**, 30 (2012) [[arXiv:1207.7235](#) [[hep-ex](#)]].
- [3] ATLAS-CONF-2013-034; ATLAS-CONF-2013-080; ATLAS -CONF-2012-135
- [4] CMS-PAS-HIG-13-005
- [5] CMS-HIG-13-015; CMS-HIG-13-019.
- [6] CMS-HIG-13-020
- [7] S. Chatrchyan *et al.* [CMS Collaboration], JHEP **1305**, 145 (2013) [[arXiv:1303.0763](#) [[hep-ex](#)]].
- [8] J. R. Ellis, M. K. Gaillard and D. V. Nanopoulos, Nucl. Phys. B **106**, 292 (1976).
- [9] M. A. Shifman, A. I. Vainshtein, M. B. Voloshin and V. I. Zakharov, Sov. J. Nucl. Phys. **30**, 711 (1979) [*Yad. Fiz.* **30**, 1368 (1979)].
- [10] A. Azatov and J. Galloway, Int. J. Mod. Phys. A **28**, 1330004 (2013) [[arXiv:1212.1380](#)].
- [11] F. Maltoni, D. L. Rainwater and S. Willenbrock, Phys. Rev. D **66** (2002) 034022 [[hep-ph/0202205](#)]; S. Biswas, E. Gabrielli and B. Mele, JHEP **1301**, 088 (2013)

- [arXiv:1211.0499 [hep-ph]]; S. Biswas, E. Gabrielli, F. Margaroli and B. Mele, arXiv:1304.1822 [hep-ph]; D. Curtin, J. Galloway and J. G. Wacker, arXiv:1306.5695 [hep-ph]; M. Farina, C. Grojean, F. Maltoni, E. Salvioni and A. Thamm, JHEP **1305**, 022 (2013) [arXiv:1211.3736 [hep-ph]]; N. Craig, M. Park and J. Shelton, arXiv:1308.0845 [hep-ph]; P. Onyisi, R. Kehoe, V. Rodriguez and Y. Ilchenko, arXiv:1307.7280 [hep-ex]; P. Agrawal, S. Bandyopadhyay and S. P. Das, arXiv:1308.6511 [hep-ph].
- [12] R. V. Harlander and T. Neumann, arXiv:1308.2225 [hep-ph].
- [13] M. Grazzini and H. Sargsyan, arXiv:1306.4581 [hep-ph].
- [14] D. B. Kaplan, H. Georgi and S. Dimopoulos, Phys. Lett. B **136**, 187 (1984); D. B. Kaplan and H. Georgi, Phys. Lett. B **136**, 183 (1984); R. Contino, Y. Nomura and A. Pomarol, Nucl. Phys. B **671**, 148 (2003) [hep-ph/0306259]; K. Agashe, R. Contino and A. Pomarol, Nucl. Phys. B **719**, 165 (2005) [hep-ph/0412089].
- [15] A. Falkowski, Phys. Rev. D **77**, 055018 (2008) [arXiv:0711.0828 [hep-ph]]; I. Low and A. Vichi, Phys. Rev. D **84**, 045019 (2011) [arXiv:1010.2753 [hep-ph]]; A. Azatov and J. Galloway, Phys. Rev. D **85**, 055013 (2012) [arXiv:1110.5646 [hep-ph]]; M. Montull, F. Riva, E. Salvioni and R. Torre, arXiv:1308.0559 [hep-ph].
- [16] A. Banfi, A. Martin and V. Sanz, arXiv:1308.4771 [hep-ph].
- [17] R. K. Ellis, I. Hinchliffe, M. Soldate and J. J. van der Bij, Nucl. Phys. B **297**, 221 (1988).
- [18] U. Baur and E. W. N. Glover, Nucl. Phys. B **339**, 38 (1990).
- [19] T. Hahn and M. Perez-Victoria, Comput. Phys. Commun. **118**, 153 (1999) [hep-ph/9807565].
- [20] R. Brock *et al.* [CTEQ Collaboration], Rev. Mod. Phys. **67**, 157 (1995).
- [21] C. J. Glosser and C. R. Schmidt, JHEP **0212** (2002) 016 [hep-ph/0209248].
- [22] B. Field, S. Dawson and J. Smith, Phys. Rev. D **69** (2004) 074013 [hep-ph/0311199].

- [23] A. D. Martin, W. J. Stirling, R. S. Thorne and G. Watt, Eur. Phys. J. C **63**, 189 (2009) [[arXiv:0901.0002 \[hep-ph\]](#)].
- [24] D. de Florian, G. Ferrera, M. Grazzini and D. Tommasini, JHEP **1111**, 064 (2011) [[arXiv:1109.2109 \[hep-ph\]](#)].
- [25] J. Alwall, M. Herquet, F. Maltoni, O. Mattelaer and T. Stelzer, JHEP **1106**, 128 (2011) [[arXiv:1106.0522 \[hep-ph\]](#)].
- [26] ATL-PHYS-PUB-2012-004
- [27] C.Grojean, E.Salvioni, M.Schlaffer, A.Weiler [[arXiv:1312.3317 \[hep-ph\]](#)] [arXiv:1312.3317 \[hep-ph\]](#). , Plenary talk by A. Weiler at [[SUSY 2013](#)], talk by C. Grojean at [[EPS 2013](#)]